

PACS numbers: 42.55.Rz; 42.65.Re; 33.80.–b; 52.50.Jm
DOI: 10.1070/QE2013v043n04ABEH015113

Laser breakdown in air at ultrahigh laser pulse repetition rates

V.V. Kononenko, T.V. Kononenko, V.P. Pashinin, V.M. Gololobov, V.I. Konov

Abstract. **Some specific features of interaction of intense femtosecond laser pulses with air at ultrahigh pulse repetition rates have been experimentally studied. Data on the dynamics of plasma cloud expansion and the plasma electron density on time intervals no longer than 10 ns are obtained by femtosecond interferometry. These data are interpreted in terms of the most likely mechanisms of ionised gas recombination. The effect of ultrahigh-frequency laser radiation on a medium was modelled by double-pulse irradiation with a short delay Δt between the pulses: from 1 ps to 11 ns. A nonmonotonic dependence of the degree of air ionisation by the second pulse on the delay time Δt is found; possible mechanisms of these dependences are discussed in terms of the processes of femtosecond radiation absorption in the residual plasma.**

Keywords: *femtosecond laser radiation, air breakdown, lasers with ultrahigh pulse repetition rate.*

1. Introduction

Constant progress in the development of laser technique has given rise to pulsed laser sources with an average output power reaching and even exceeding ~100 W at a pulse repetition rate of ~100 MHz [1, 2]. At the same time, it is known that, even at rates of ~4 kHz [3], residual excitation effects start manifesting themselves during ablation of solids, when the target or evaporated material do not have enough time to completely relax by the arrival of the next pulse; this circumstance significantly affects the steady-state regime of target ablation.

To date, the gas dynamics of target material vapour and the influence of the environment on this dynamics have been studied well. A well-established term 'fireball' [4, 5] is used for a long-lived (~ 1 ms) cloud of hot weakly ionised gas, which forms a low-pressure region near the surface; this region promotes, in particular, a higher ablation rate. From the practical point of view, this phenomenon may have negative consequences: erosion etching of surfaces and deterioration of laser processing quality [6].

However, there are two gaps in the studies in this field. This has become clear to date, with the development of femtosecond lasers providing a peak power above 12 MW at a pulse repetition rate of ~100 MHz [2]. Under these conditions, sufficiently tight focusing may yield an intensity of $\sim 5\times10^{14}$ W cm^{-2}, at which air breakdown occurs even in the absence of an absorbing target and, obviously, nonlinear processes accompanying light absorption and laser beam propagation become very important. In addition, the characteristic times we are interested in are currently ~10 ns or less, with allowance for the maximum pulse repetition rate implemented in high-power laser sources.

In this paper, we report the results of studying the specific features of interaction of intense femtosecond laser pulses with air at ultrahigh (~100 MHz) pulse repetition rates. We used two supplementing approaches: study of the relaxation dynamics of the air plasma formed by a single laser pulse by femtosecond interferometry and analysis of the specific features of air ionisation by two subsequent pulses with a time delay varied in the range from 1 ps to 10 ns, which allowed us to estimate the effect of high-frequency laser irradiation in the first approximation.

2. Experimental

The laser system we used included a Tsunami Ti: sapphire laser (Spectra Physics) with a working wavelength of 800 nm. A Spitfire regenerative amplifier (Spectra Physics) provided a train of pulses with a maximum energy of 1000 μJ at a repetition rate of 1 kHz. The irradiation results were visualised using the probe-beam technique (Fig. 1). Most part of radiation after the splitter (the excitation pulse) passed through a Michelson interferometer to form two pulses of equal energy with a controlled time delay. Then the laser beam was focused in air by an aspherical lens with a focal length of 8 mm. The Gaussian beam diameter in the focal plane of the lens was ~1.7 μm at a level of 1/e. The intensity on the beam axis was $\sim 2\times10^{15}$ W cm^{-2}. The variation of delay in wide limits, from several hundreds of femtoseconds to several tens of nanoseconds, made it possible to model the ultrahigh-frequency (not less than 100 MHz) irradiation regime, which is currently difficult to implement in practice.

The probe beam passed through the delay line and transilluminated the excited region from aside. The image of the region exposed to intense laser irradiation was projected on a CCD matrix plane with a magnification of ~30. Then, the image was digitised and processed to obtain information about the state of the irradiated region.

The main tool yielding quantitative information about the state of the material during and after laser irradiation was femtosecond interferometry. A Sagnac interferometer was located between the projection objective and the matrix on

V.V. Kononenko, T.V. Kononenko, V.P. Pashinin, V.M. Gololobov, V.I. Konov A.M. Prokhorov General Physics Institute, Russian Academy of Sciences, ul. Vavilova 38, 119991 Moscow, Russia; e-mail: vitali.kononenko@nsc.gpi.ru

Received 24 December 2012
Kvantovaya Elektronika **43** (4) 356–360 (2013)
Translated by Yu.P. Sin'kov

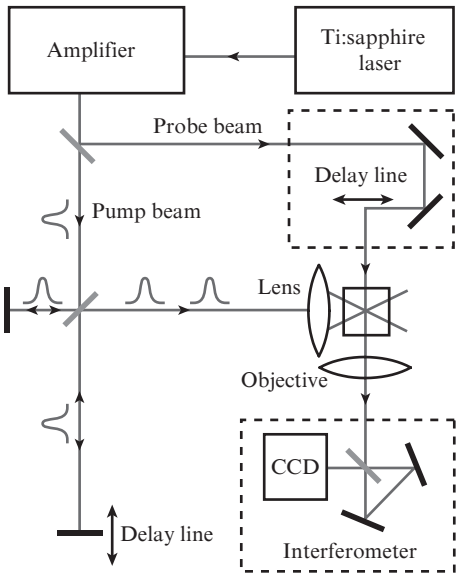

Figure 1. Experimental setup.

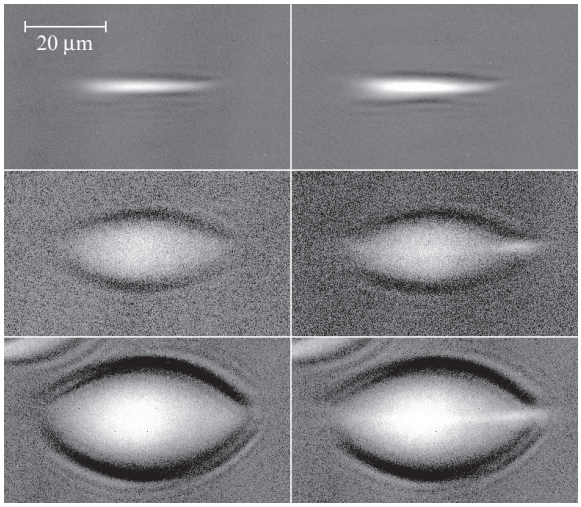

Figure 2. Interference photographs of a laser spark in air for single- and double-pulse irradiation (on the left and right, respectively). The delays between the first and probe pulses are (from top to bottom) 2 ps, 1 ns, and 11 ns. The second excitation pulse (on the right) passed through the caustic 1 ps before the arrival of the probe pulse.

which interference of two beams was observed; each beam contained a local phase perturbation, caused by the change in the refractive index n in the irradiated region. Since the width of interference fringes significantly exceeded the perturbed-region size, their shift with a change in the refractive index led to a local change in the image brightness, thus making it possible to calculate Δn. In the figures presented below, higher and lower brightness levels correspond, respectively, to reduced and increased n values. Minimisation of mechanical vibrations and accumulation of photographs obtained under the same irradiation conditions with their subsequent averaging allowed us to measure the electromagnetic wave phase $\delta\phi$ in the probe beam with sensitivity better than 10^{-2}.

3. Results and discussion

As was noted above, the key factor determining the physics of interaction between a pulsed laser beam with an ultrahigh pulse repetition rate and a medium is the residual excitation of the material in the irradiated region. The 'excitation' is considered to be the laser-induced change in the state of the material, primarily the degree of its ionisation and the degree of deviation of the energy distribution of charged particles from equilibrium, as well as the temperature, partial pressures, and local densities of the plasma components. Obviously, to understand the specific features of high-frequency pulse laser processing, one needs detailed information about the relaxation processes occurring in the medium.

3.1. Relaxation of air breakdown plasma by femtosecond laser pulses

The microbreakdown photographs (Fig. 2) show that the initially ionised region, formed during the pulse, has a diameter of ~6 μm and a length ~60 μm, which are determined by the degree of field localisation in the beam caustic. Then, due to the diffusion of radiation-heated electrons, the plasma cloud begins to expand and reaches ~50 μm in diameter after 11 ns. At these sizes, as can be seen in Fig. 2 (lower photographs), even the interference image of the spark that is present in the second interferometer arm partially enters the frame. Note also the occurrence of a relatively narrow layer with a positive change in the refractive index around the expanding cloud. Obviously, it is related to the dynamic air compression by the shock-wave pressure.

Figure 3 shows an experimental time dependence of the spark radius, which can be approximated by the function

$$R(t) = R_0\sqrt{1+\frac{t}{\tau}}, \tag{1}$$

where $R_0 = 2.7$ μm is the initial size of the plasma cloud and $\tau = 140$ ps is a time constant. A similar dependence is given by the model of point explosion [7]:

$$R(t) \propto t^a, \tag{2}$$

where $a = 0.5$ in the case of instantaneous energy release along a straight line – the case of cylindrical symmetry, which is,

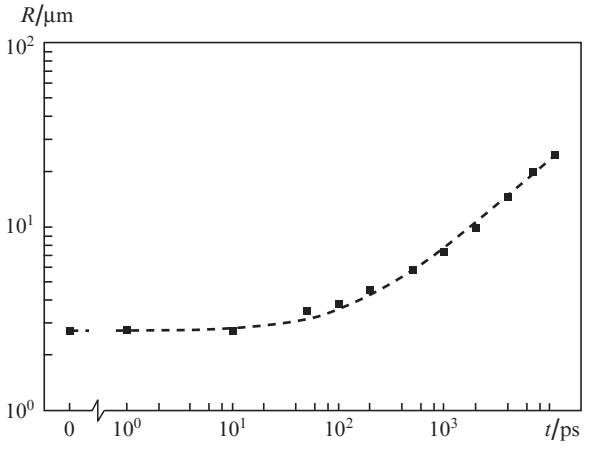

Figure 3. Temporal dynamics of the size of the plasma cloud in air: (squares) experimental data and (solid line) dependence (1).

obviously, most close to the case under consideration. The experimental dependence (1) differs from the theoretical one (2) by the presence of a correction term on the order of τ = 140 ps under the radical sign, which is due to the following factors: in a real experiment energy is released along the cylinder of finite radius R_0 and the front of explosive wave starts propagating not from the zero point. Note that the shock-wave speed, being initially 10^6 cm s^{-1}, decreases to 10^5 cm s^{-1} after 11 ns, i.e., almost to the speed of sound in air.

The expansion of the plasma cloud with time significantly changes the shape of the initial distribution of plasma density in space, which can be seen well in the corresponding profiles $N(r)$ (Fig. 4). The carrier concentration N was calculated from the Drude formula, which is believed to be a good approximation in the case under consideration (classical, almost ideal plasma):

$$\varepsilon = 1 - \frac{4\pi e^2 N}{m_e \omega^2},$$

where ε is the permittivity for an electromagnetic wave with a frequency ω; e is the elementary charge; and m_e is the electron mass. The profiles of local perturbation of the refractive index of ionised air were obtained, in turn, from the interference images using the inverse Abel transform. Note that the transverse profile significantly changes its shape during cloud expansion: from a Gaussian-like in the beginning to a plateau-like in the late stages of expansion. The spread of material is obviously nonuniform: first (after 1 ns) a relatively rarefied region arises at the centre of the spark, which is replaced with a compacted region after 11 ns (Fig. 4).

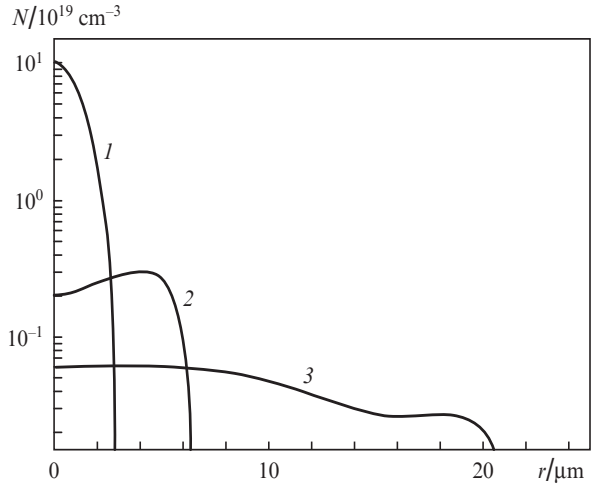

Figure 4. Transverse profiles of local carrier concentration during expansion and relaxation of a laser spark in air at delays Δt = (*1*) 1 ps, (*2*) 1 ns, and (*3*) 11 ns.

Obviously, the thermal diffusion expansion of the electron cloud decreases the local carrier concentration in the course of time. It is also clear that the electron–ion recombination leads to the same effect. The relative contribution of these mechanisms to the change in the carrier concentration can be estimated from the dynamics of $N(t)$, which is shown in Fig. 5 for a point on the laser beam axis. An interesting feature of this dependence is the continuation of ionisation of molecules in air after the end of the laser pulse for approximately 10 ps. A similar effect was observed by Butin et al. [8], who explained it by the possibility of significant laser overheating of some part of electrons, which should lead to accumulation of light energy in the form of carrier kinetic energy and, therefore, delay its dissipation. However, in view of the purpose of our study, the further dynamics of N is much more interesting.

As follows from Fig. 5, the local carrier concentration is described fairly well by the dependences $N \propto 1/t$ at t = 10–1000 ps and $N \propto 1/\sqrt{t}$ at $t > 1$ ns. An attempt to describe this dynamics in terms of heated plasma expansion turned out to be inconsistent. Figure 5 presents a dashed curve, which is obtained by simulating the plasma cloud expansion on the assumption that it occurs uniformly, according to the formula $N(t) = N(t_0)R^2(t)/R^2(t_0)$, where $N(t_0)$ is the electron concentration in the centre of the spark at the initial instant (t_0 = 10 ps); $R(t)$ is the spark radius, in correspondence with the data in Fig. 3. It can clearly be seen that the electron concentration decreases in fact much more rapidly than should according to the simple model of uniform cylindrical expansion. It is also of little use to discuss the possible influence of the material spread inhomogeneity, because the experimental values differ from calculated ones by a factor of 10 at t = 1 ns, which is much larger than the measured inhomogeneity of the carrier concentration in the plasma cloud (Fig. 4). Thus, the temporal dynamics of plasma density in air is mainly determined by the electron–ion recombination.

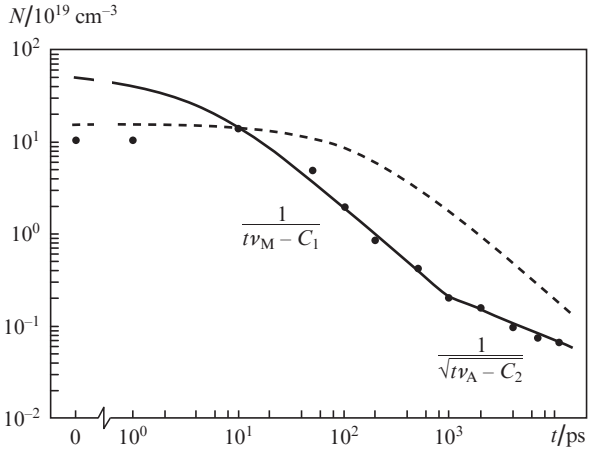

Figure 5. Dynamics of plasma density in the centre of the breakdown induced by a single laser pulse: (circles) experimental data, (solid line) recombination, and (dashed line) expansion of plasma cloud.

Following numerous works, where recombination processes in classical plasma were investigated in detail (see, for example, [9, 10]), we found that the experimental data can satisfactorily be described in terms of two main mechanisms: dissociative recombination, which dominates in the case of molecular gases, and three-particle recombination, which is dominant for atomic gases. A characteristic feature of the former is that the collision of a diatomic or polyatomic M_2^+ (O_2^+, N_2^+, H_2O^+, etc.) with an electron can be inelastic, in which the kinetic energy is transformed into the energy of internal degree of freedom, allowing for fulfilment of the conservation laws and providing excitation and recombination of molecules in the long run. The corresponding reaction has the form

$$M_2^+ + e^- \rightarrow 2M,$$

and its kinetic equation can be written as $dN_M/dt = -v_M N_M^2$, where v_M is the reaction probability. A solution to this equation is

$$N_M(t) = \frac{1}{tv_M - C_1}, \quad (3)$$

where C_1 is a constant determined by the initial degree of air ionisation.

In the case of single-atom gases in the air composition (Ar, Ne), the characteristic recombination reaction calls for a third particle (which is generally an electron due to the larger thermal electron velocity); therefore, the reaction occurs much more slowly:

$$A^+ + e^- + e^- \rightarrow A + e^-.$$

The corresponding kinetic equation has the form $dN_A/dt = -v_A N_A^3$, and its solution is

$$N_A(t) = \frac{1}{\sqrt{tv_M - C_2}}. \quad (4)$$

The obtained solutions (3) and (4) are presented in Fig. 5; they show that the dynamics of the electron concentration is completely described by the above-considered recombination mechanisms. Three-particle recombination begins at the very start of the ionisation of the medium; however, since polyatomic gases dominate in air, recombination of single-atom gases is pronounced only after ~1 ns, when the reaction for the polyatomic component actually stops. Note that at this instant the initial plasma density decreases by a factor of about 100; i.e., ~1% of all ionised molecules are retained, which clearly correlates with the percentage of noble gases in air. Note another interesting fact. The analysis performed showed that the recombination is sufficiently fast and significantly decreases the carrier concentration in air for the first 10 ps after the end of the laser pulse. Approximation of the recombination dependence makes it possible to estimate the concentration of electrons produced by ionisation. It is not $\sim 1.5\times10^{20}$ cm^{-3} (see Fig. 5) but much larger: about 4×10^{20} cm^{-3}; note that this 'additional' ionisation occurs fairly slowly after the end of the pulse (for a time of ~10 ps), presumably due to the above-mentioned impact ionisation by hot electrons [8].

Thus, our experiments showed that, after the laser excitation, the state of the air medium (primarily, the degree of ionisation and the material density) dramatically changes for few nanoseconds. Even after 10 ns we deal with almost neutral and rather dilute hot gas; i.e., one can speak about the formation of a 'fireball' that will slowly cool down for several hundreds of microseconds [3].

3.2. Irradiation by two pulses

We performed experiments with air ionisation by the second pulse, delayed with respect to the first one by a time interval varied from 1 ps to 11 ns (characteristic air plasma relaxation time). Figure 2 shows (on the right) interference images of the excited region, which were made at a fixed time interval (1 ps) after the second pulse transmission. Under these conditions, the relaxation and recombination processes induced in the plasma by the second pulse can be neglected. Obviously, the plasma cloud did not have enough time to expand and was observed in all photographs as a narrow long region, coinciding with the laser caustic. It can be seen that, at short delays (~1 ps) between excitation pulses (upper photographs), the degree of air ionisation after the transmissions of the first and second pulses are comparable. At the same time, at longer delays the concentration of the plasma induced by the second pulse dramatically decreases. At a delay of ~1 ns the induced variation in n was very small (at the noise level in the interference photographs).

Note that the suppression of air ionisation by the second pulse is clearly localised in space within the region occupied by the fireball. Figure 6 shows a microscopic breakdown in air, obtained as a result of double-pulse irradiation with an 11-ns delay, i.e., under the conditions similar to those in Fig. 2 (the photograph in the bottom right corner). In this case, the propagation direction of the second pulse was varied by rocking one of the mirrors to make the beam axes diverge. As a result, the moment the second-beam caustic shifted so as to leave partially (Fig. 6, on the right) or completely (Fig. 6, on the left) the plasma region formed by the first pulse, the ionisation efficiency was recovered.

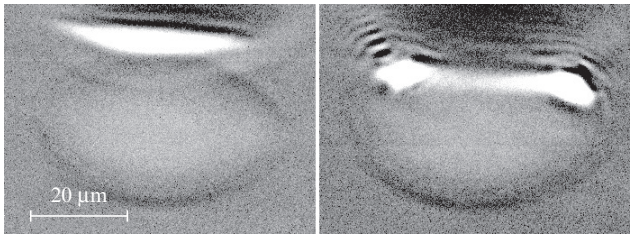

Figure 6. Interference image of air breakdown induced by irradiation by two pulses with a delay of 11 ns at vertical displacement of the second-beam caustic with respect to the first beam.

There is also a clear tendency to a change in the shape of the plasma cloud induced by the second pulse. Figure 2 shows that, at nanosecond delays between the pulses, the laser spark for the second pulse is longer than for the first one: breakdown develops mainly on the beam axis, in the region occupied by the front of the shock wave produced by the expanding fireball.

The change in the electron concentration after the second pulse as a function of the delay between the pulses is presented in Fig. 7. It can be seen that at delays shorter than 100 ps the concentration of the free carriers induced by the second pulse is much lower (by a factor of more than 4) than the concentration of the carriers induced by the first pulse (see Fig. 5). This circumstance is not related to the relaxation processes but is caused (as showed our experiments, which are not described here) by gradual saturation of the ionisation rate with an increase in the pulse energy. An increase in the delay time to several nanoseconds leads to a sharp decrease in the ionisation efficiency (to values comparable with the noise). With a further increase in the delay the plasma induced by the second pulse arises again, although remains a very weak additive to the spark formed by the first pulse. This process may determine (specifically, increase) the efficiency of laser irradiation of materials under the following conditions: optical air breakdown occurs near the irradiated surface and the laser pulse repetition rate reaches 100 MHz.

This effect of ionisation suppression in an expanding plasma cloud was qualitatively explained in [3] in terms of

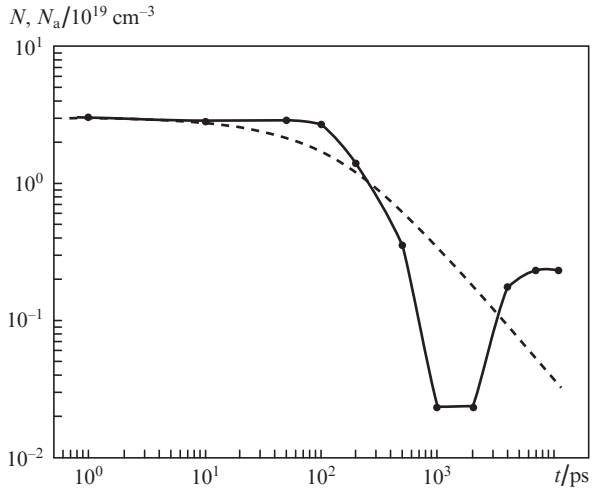

Figure 7. Additional air ionisation, induced by the second laser pulse passing through the breakdown region, as a function of the delay between the pulses: (circles) charge-carrier concentration N, measured in the breakdown region, and (dashed line) calculated concentration of gas molecules, N_a, in the expanding cloud.

sharp decrease in the gas density in the breakdown region, which results in the corresponding decrease in the density of newly ionised molecules. The fact that ionisation is suppressed at delays between pulses longer than 100 ps, when the shock wave leaves the irradiated region and the plasma begins to expand, is in agreement with this explanation. However, the observed degree of suppression of the plasma formation and the local gas density in the fireball are much less consistent. This can be seen well in Fig. 7, which presents, along with the experimental data, a time dependence of the gas molecule concentration, calculated from the velocities of material spread (see Fig. 3), on the assumption that the density of the medium is constant in the plasma cloud. Obviously, to gain a deeper insight into the processes of photoionisation of preionised gas, one must take into account at least the following important circumstances.

First, according to the theory of point explosion [7], it is a rarefaction that first arises in the breakdown centre during supersonic gas expansion. Then the back pressure of the environment gives rise to a back gas flow to the centre of symmetry and, therefore, to relative air compression in the explosion centre [11]. This behaviour can qualitatively explain the observed dynamics of air ionisation efficiency for the second pulse (Fig. 7). Moreover, the experimental profiles of the electron (and, therefore, ion) concentration have the same shape (see Fig. 4).

Second, it is necessary to take into account the rather fast recombination of polyatomic ions, which, obviously, should facilitate the breakdown development with an increase in the delay between the pulses. However, we should note that the atomic nitrogen and oxygen arising after dissociation have in general an electronic structure significantly differing from the corresponding molecular compounds. In addition, the tunnel ionisation of these compounds in strong fields has been poorly studied [12].

Finally, the optical properties of plasma (in particular, absorption) depend on its temperature and density: the efficiency of inverse bremsstrahlung absorption and impact ionisation is determined by the temperature dependences of the electron–ion scattering cross section.

4. Conclusions

We experimentally investigated the processes of relaxation in femtosecond laser plasma and the efficiency of repeated laser breakdown in a time interval of 0–11 ns in an air medium that did not completely relax. Significant differences were revealed in the localisation of plasma cloud and degree of its ionisation in the optical gas breakdown by the first and second pulses with a time delay of 0.1–10 ns. It was shown that a specific feature of fast (100 fs) microscopic breakdown is that the gas dynamics of this spark in air is described very well by the point explosion model. It was also demonstrated that the main recombination processes determining the temporal dynamics of the degree of air ionisation are dissociative recombination (in the case of molecular components) and three-particle recombination (for atomic components).

Acknowledgements. This work was supported by the programme 'Extreme Light Fields and Their Applications' of the Presidium of the Russian Academy of Sciences and the Russian Foundation for Basic Research (Grant No. 11-02-12242).

References

1. Song R., Hou J., Chen S., Yang W., Lu Q. *Appl. Opt.*, **51** (13), 2497 (2012).
2. Eidam T., Hanf S., Seise E., Andersen T.V., Gabler T., Wirth C., Schreiber T., Limpert J., Tünnermann A. *Opt. Lett.*, **35** (2), 94 (2010).
3. Klimentov S.M., Pivovarov P.A., Konov V.I., Braitling D., Dausinger F. *Kvantovaya Elektron.*, **34** (6), 537 (2004) [*Quantum Electron.*, **34** (6), 537 (2004)].
4. Askar'yan G.A., Rabinovich M.S., Savchenko M.M., Stepanov V.K. *Pis'ma Zh. Eksp. Teor. Fiz.*, **5** (5), 150 (1967).
5. Prokhorov A.M., Konov V.I., Ursu I., Mikheilesku I.N. *Vzaimodeistvie lazernogo izlucheniya s metallami* (Interaction of Laser Radiation with Metals) (Moscow: Nauka, 1988).
6. Breitling D., Ruf A., Berger P.W., Dausinger F.H., Klimentov S.M., Pivovarov P.A., Kononenko T.V., Konov V.I. *Proc. SPIE*, **5121**, 24 (2003).
7. Sedov L.I., Korobeinikov V.P., Markov V.V. *Trudy MIAN SSSR*, 175, 178 (1986).
8. Bukin V.V., Garnov S.V., Malyutin A.A., Strelkov V.V. *Kvantovaya Elektron.*, **37** (10), 961 (2007) [*Quantum Electron.*, **37** (10), 961 (2007)].
9. Hahn Y. *Rep. Prog. Phys.*, **60** (7), 691 (1997).
10. Kampfrath T., Gericke D.O., Perfetti L., Tegeder P., Wolf M., Frischkorn C. *Phys. Rev. E*, **76** (6), 066401 (2007).
11. Korobeinikov V.P. *Trudy MIAN SSSR*, **119**, 3 (1973).
12. Seideman T., Ivanov M.Yu., Corkum P.B. *Phys. Rev. Lett.*, **75** (15), 2819 (1995).